International Journal of Steel Structures (2022) 22(5):1341–1358
https://doi.org/10.1007/s13296-022-00645-8

Online ISSN 2093-6311
Print ISSN 1598-2351

Artificial Neural Network (ANN) Based Prediction of Ultimate Axial Load Capacity of Concrete-Filled Steel Tube Columns (CFSTCs)

Cigdem Avci-Karatas[1]

Received: 24 March 2021 / Accepted: 15 July 2022 / Published online: 5 August 2022

Abstract

Concrete-filled steel tube columns (CFSTCs) are preferred due to enhanced ductility and energy absorption. The capability of an artificial neural network (ANN) based analytical model on estimating the ultimate load capacity of circular CFSTCs under axial loadings has been investigated in this study. To provide a better prediction in modeling, 150 comprehensive experimental data were obtained from circular CFSTC's geometrical and mechanical properties, such as height, diameter, thickness, the yield stress of steel, unconfined concrete strength, Young's modulus of steel and concrete, etc., were examined. The backpropagation-training practice available in ANN was used to update the weights of each layer based on the network output error. For feedforward–backpropagation, the Levenberg–Marquardt algorithm was employed. The effectiveness of the ANN model was developed using general-purpose software MATLAB® by training and predicting the ultimate load capacity of circular CFSTCs. Finally, about 75% of the data were used for ANN training, and the remaining 25% was used for testing the ANN model. The results show that the predicted values of ultimate load capacity using the ANN model agree well with that of the corresponding experimental observations, and the percentage difference is about ± 10%. Additionally, a new engineering index, a20-index, was predicted to further verify the reliability of the model. The findings of this article are new and will significantly contribute to the existing technology of ANN-based modeling in composite construction.

Keywords Concrete-filled steel tube column · Composite structures · Ultimate axial load capacity · Artificial neural network (ANN) · Statistical modeling tool · Soft computing method

Abbreviations

D	Outer diameter of steel tube
d_k	Direction vector
E	Output error function
E_c	Young's modulus of concrete
E_s	Young's modulus of steel,
f_c	Unconfined concrete compressive strength
f_y	Yield strength of structural steel
g	Nonlinear activation function
L	Length of CFSTC
$m20$	No. of samples whose value of the ratio experimental to predicted lies between 0.8 and 1.2
N	No. of dataset sample
P_u	Ultimate axial load capacity
P_u^E	Experimental ultimate load
P_u^{ANN}	Predicted ultimate load in the ANN-based model
P_u^{MARS}	Predicted ultimate load in the MARS-based model
P_u^{RVM}	Predicted ultimate load in the RVM-based model
R^2	Coefficient of determination R-squared
t	Wall thickness of steel tube
w_k	Individual weight at epoch k
$x_i^a i^{th}$	Component of the input vector before normalization
$x_i^n i^{th}$	Component of the input vector after normalization
x_i^{max}	Maximum value of all the components of the input vector before the normalization
x_i^{min}	Minimum value of all the components of the input vector before the normalization
η	Learning rate
ξ	Confinement factor

✉ Cigdem Avci-Karatas
cigdem.karatas@yalova.edu.tr

[1] Department of Transportation Engineering, Faculty of Engineering, Yalova University, Yalova 77200, Turkey

1 Introduction

The common form of composite elements in construction is the steel–concrete composite elements, which are widely used in the modern construction industry because of the mechanical and economic advantages provided by the composite techniques (as examined by Avci-Karatas et al., 2018, 2019; Celik et al., 2015; Ghamari & Johari-Naeimi, 2021; Hoveidae & Radpour, 2021; Talyan et al., 2021). The joining of two structural materials' stronger properties, and hence, decreasing their weakness has resulted in a superior performance against the individual use of those materials. Steel–concrete composite elements such as composite columns (i.e., completely/partially encased and filled composite columns), composite beams, and composite slabs use compressive strength of concrete alongside the resistance to tension of steel, and when tied together this results in a highly efficient and lightweight unit that is commonly used for structures such as multi-story buildings and bridges. As known to be composite members, concrete-filled steel tube columns (CFSTCs) offer many structural benefits such as high strength, favorable ductility, and large energy absorption capacities, incorporating the advantages of steel and concrete. The concrete strength is increased due to the confinement effect provided by the steel tube. Moreover, the inward local buckling of the steel tube is prevented by core concrete, which helps increase the load-bearing capacity and enhances the ductility. CFSTCs also offer excellent static and seismic performances. Because of these advantages, CFSTCs are commonly used in buildings, bridges, towers, substations, etc. CFSTCs were also used as bridge piers in Japan and Europe (Abdelkarim et al., 2015; Kitada, 1998). Further, CFSTCs were employed for retrofitting purposes in earthquake-prone areas (Sakino & Sun, 2000). Soman and Chandrakumar (2018) found that the ultimate load of reinforced concrete (RC) square short/stub columns strengthened with glass fiber reinforced polymer (FRP) under axial loading and proposed an analytical model to predict the ultimate load. Chalioris et al. (2020) conducted experiments on shear critical T-shaped RC beams strengthened with epoxy bonded carbon FRP and found that the enhanced the shear resistance. It was mentioned that brittle failure mode was observed with delayed debonding due to mechanical anchor. Moreover, the shear capacity of retrofitted beams was estimated using different codes. It was mentioned in the literature that the strength or failure load of CFSTCs depends on material properties and steel ratio (Schneider, 1998; O`Shea and Bridge 2000; Johansson & Gylltoft, 2002; Sakino et al., 2004; Han & Yao, 2004; Han et al., 2005). Various cross-sections of CFSTCs such as circular, square, and rectangular were employed for the investigations. Several investigations were performed on CFSTCs having various grades of concrete (for instance, Uy, 2001; Liu et al., 2003; Liu et al. 2005; Lue et al., 2007; Yu et al., 2008; Aslani et al., 2015). The load-carrying capacity of CFSTCs with several grades, such as 30, 60, and 100 MPa was investigated depending on the effects of various steel tube thickness by Giakoumelis and Lam (2004). Several experimental findings indicated that Specification for Structural Steel Buildings (ANSI/AISC 360-16) (2016), Eurocode 4 (EC4) (2004), American Concrete Institute (ACI), and Australian Standards (AS) estimate conservatively the axial load capacities of normal and high-strength CFSTCs. Ellobody et al. (2006) conducted parametric studies on circular normal and high-strength CFSTCs. From this study, it was observed that the design strengths obtained by ACI and AS codes are found to be conservative, but EC4 commonly overestimates. Lam and Gardner (2008) carried out systematic studies on the behavior of axially loaded square and circular CFSTCs with concrete compressive strengths varying from 30 to 100 MPa. It was found that EC4 and Architectural Institute of Japan (AIJ) design codes yielded conservative and can be safely applied to normal strength CFSTCs. Xiong et al. (2017) performed extensive investigations on CFSTCs with high and ultrahigh strength concrete.

A general observation is that it takes a considerable amount of time and effort to carry out experiments. Further, numerical simulation requires accurate modeling to represent the realistic behavior of experimental findings. Several statistical models were proposed in the literature to train the data and predict the output. The meta-models (MMs) are, in general, data-driven models that will be useful for simulating the input/output behavior of the system. Training and testing are the two essential basic steps to construct a MM. The training corresponds to fitting a model based on the relations between the dependent and independent variables, and testing involves comparing the predictions of MM to the actual response. There are several advanced statistical models or MMs such as artificial neural networks (ANNs), Gaussian process regression (GPR), least-squares support vector machine (LS-SVM), multivariate adaptive regression splines (MARS), relevance vector machine (RVM), and extreme learning machine (ELM), etc., (Yuvaraj et al., 2013; Yuvaraj et al., 2014; Mansouri et al., 2016; Dutta et al., 2017; Kaur et al. 2017; Mansouri et al., 2017; Prasanna et al., 2018; Murthy et al., 2019; Avci-Karatas, 2019; Gholampour et al., 2020). Each regression model has its own merits and limitations.

ANN is a statistical modeling tool that originated from the inspiration of biological neural networks. Artificial neurons are interconnected to each other, where processing required data using a connectionist approach to estimation. Several studies were reported in the literature on ANN.

Haque and Sudhakar (2002) predicted fracture toughness and tensile strength of micro-alloyed steel using ANN. The fracture parameters of concrete were also evaluated by Ince (2004) using ANN, and compared to the findings of the two-parameter model (TPM) and ANN. Akbas et al. (2011) predicted the seismic-induced demands on column splices by ANN and found the predictions are to be satisfactory. Duan et al. (2013) examined ANN's applicability to estimate the compressive strength of recycled aggregate concrete. Cheng and Cao (2013) proposed a novel ANN model to estimate the shear strength of RC deep beams. Chithra et al. (2016) developed multiple regression analysis and ANN models to estimate the compressive strength of high-performance concrete made up of nanoscale silica and copper slag. Behnood and Golafshani (2018) estimated the compressive strength of silica fume concrete using ANN. It is a fact that conducting several experiments takes a considerable amount of time and effort.

To design the optimum experiments, quick and preliminary information will be useful. Several models based on the concept of ANN, SVM, RVM, MARS, GPR, etc., were developed to predict the responses of structures/structural components under various loadings. Input data are to be prepared very carefully by identifying the dependent and independent variables. Le (2020) highlighted a machine-learning (ML) model on GPR to estimate the load capacity of square CFSTCs. The nonlinear characteristics of CFSTCs (e.g., length and thickness of steel tube, the length-to-diameter ratio of composite columns, concrete strength, etc.). Besides, an artificial intelligence (AI) model was provided by Ngo et al. (2021) using support vector regression (SVR), and grey-wolf-optimization (GWO) to guess the ultimate load capacity of circular CFSTCs. In the earlier studies, Avci-Karatas (2019, 2021) proposed models to estimate the load capacity of axially loaded circular CFSTCs based on the concepts of MARS and RVM. In this analytical research relevant to engineering practice, it is proposed to develop an alternative statistical model based on ANN's concept for estimating the ultimate load capacity of circular CFSTCs. This will provide new insight into the work of CFSTCs. In this way, the difference and concluding remarks derived from the current study will be highlighted concerning the MARS-based model, and RVM-based model in the previous studies of Avci-Karatas (2019, 2021).

In this study, 150 experimental data and results of circular CFSTCs were collected from previous studies. The data cover variations in steel yield strength, concrete compressive strength, geometry, and material properties of circular CFSTCs. The novelty of this research based on the current requirements in the construction industry is that the kind of comprehensive data assessed here is used on the prediction of ultimate load capacity of circular CFSTCs through AI tools and soft-computing technology. It should be noted that applying this concept in civil/structural engineering is limited in the literature. About 75% of the total data have been used for training and the remaining data has been used to verify the models. In deep physical and engineering meaning, a new engineering index, denoted as the $a20-$index, which was proposed by Asteris and Mokos (2020) was predicted to verify the reliability of the model further. This paper, with new quantitative and qualitative results falls within the scope of computational structural engineering and deals with a topic still open to question since the existing published works in this field are limited.

To positively address the researchers in the field, a comparison of the results of existing analytical models, previously provided by Avci-Karatas using the same experimental data in Avci-Karatas (2019) for the MARS-based model and Avci-Karatas (2021) for the RVM-based model, was presented regarding the superiority or advantages of the ANN-based modeling and added as Sect. 5. Especially, the load capacity calculations of composite columns have been the subject of ANSI/AISC 360-16 and EC 4 design specifications, including capacity calculations for CFSTCs. Here, these specification formulas were defined to show the effect of parameters on the capacity of CFSTCs (Al-eliwi et al., 2017). Thus, considering true parameters in a successful model, as proposed in this study, assured the strong estimations, and increased the applicability of the proposed formula in the design of axially loaded circular CFSTCs.

After providing a relevant literature review in this section, the rest of the paper is arranged as follows: Sect. 2 illustrates the experimental investigations of circular CFSTCs, Sect. 3 presents the structure and implementation of the performed nonlinear ANN algorithm-based machine learning, and Sect. 4 presents the modeling process about the development of ANN-based models to predict the load capacity of CFSTCs with circular sections under axial loadings, and the validation check studies. The prediction of the ultimate axial load capacity of circular CFSTCs using various analytical models was evaluated through MARS, RVM-based models, and compared with the developed ANN-based model in Sect. 5. Finally, Sect. 6 summarizes study findings and provides study limitations.

2 Experimental Investigations of Circular CFSTCs

Several experimental investigations were reported in the literature on the performance of circular CFSTCs under axial compression loadings. The test configuration considered herein is schematically given in Fig. 1. The loading type in the experimental setup of monotonic validation tests was conducted for short/stub concentrically loaded columns. From the wide literature review, it was observed that the

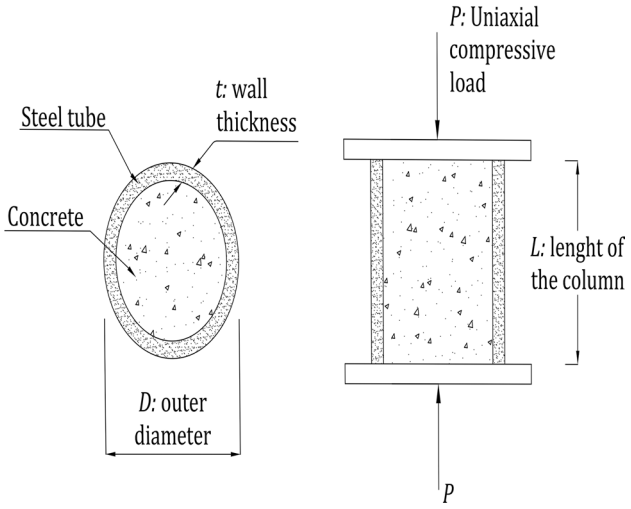

Fig. 1 Geometrical configuration of circular CFSTCs

ultimate axial load capacity, P_u, depends on various factors, such as (1) outer diameter of steel tube, D, (2) wall thickness of steel tube, t, (3) unconfined concrete compressive strength, f_c, (4) Young's modulus of concrete, E_c, (5) yield strength of structural steel, f_y, (6) Young's modulus of steel, E_s, (7) length of CFSTC, L, and (8) confinement factor, ξ. Experimental data for 150 stub circular CFSTCs were gathered from 22 several published references and will be trained to develop and verify the ANN model. Table 1 presents the geometrical parameters (namely, cross-section properties), material strength properties of concrete and steel, and failure load of various circular CFSTCs with different confinement factors under axial load. The dataset has wide-ranging column and test specimens parameters, varying from normal to high yield strength steels (f_y= 186–853 MPa), from normal concrete strength to ultra-high-strength concrete (f_c = 18–193 MPa), the outer diameter of circular sections (D = 60–450 mm), the ratio of the outer diameter to the thickness (D/t = 17–221), and the ratio of the length to the outer diameter (L/D = 1.8 − 4.9), respectively. In the definition of short and long CFSTCs, ANSI/AISC 360-16, and EC4 are completely different, therefore, the term "short " and "long" are classified according to the L/D ratio, where the "short" is defined as a specimen with L/D ratio less than or equal 4. In this paper, the investigated experimental data for the CFSTCs were evaluated as stub columns since the data sourced from the stub concentrically loaded columns. As given in Table 1, these parameters cover adequately wide practical ranges. Ekmekyapar and Al-Eliwi (2016) examined the capacity and confinement of CFSTCs with three L/D ratios, two D/t ratios, three concrete compressive strength levels, and two steel qualities. The results showed that the L/D ratio is a crucial parameter that has a direct impact on the column capacity, while D/t and ξ does not have a direct impact on the performance of CFSTCs (Ekmekyapar and Eliwi 2016). However, the only parameter that makes the load capacity of this type of composite column exceeds the typical stub column capacity is the effect of confinement, ξ. As the concrete in the circular tube is subjected to circular tension under sufficient ξ, the concrete compressive capacity increases. The other parameters that also affect ξ include D/t ratio, concrete strength, and steel strength. The aim of the developed model in this research is to provide a unique approach to obtain decreasing errors, complexity, and reducing convergence of scattering amplitudes of numerical results to experimental ones. To do so, it can be an alternative to experimental studies and to estimate the ultimate load capacity of circular CFSTCs. It can be noted from Table 1 that E_c varies between 17810 and 66000 MPa and E_s varies in the range of 177000–213000 MPa. These variations (e.g., including D/t and ξ, etc.) have been considered while producing model processes to increase the possibility of obtaining a stronger model. Note that the steps of typical regression analysis are schematically diagramed in Fig. 2. The regression algorithm requires proper input and the associated meta-parameters. Each regression algorithm assumes the specific parameters related to the anticipated model. A vector of the model parameter in the output of any algorithm can be suggested by minimizing an error measure on the training data.

3 Artificial Neural Networks (ANNs)

More detailed information about ANNs, the methodology, training, and validation of the data has been explained in the earlier studies (Haque & Sudhakar, 2002; Ince, 2004; Kamarthi & Pittner, 1999). An overview of soft-computing approaches about the ANN concept is briefly summarized as follows.

3.1 Feedforward-Backpropagation Neural Networks

In feedforward networks (FFNs), the signals will travel in one direction from the input neurons to the output neurons. The inference is that the output of any layer does not affect that same layer. Feedforward ANNs are straightforward networks contecting inputs with outputs. FFNs are widely used in pattern recognition. It can also be called a top-down approach. The information transfer/distribution is parallel for all nodes of the succeeding layer. Figure 3 describes the FFNs, typical three-layer feedforward multi-layer perceptron network architecture with i, j, and o neurons being the input, hidden, and output layers, respectively. Figure 3 consists of the activation function, weights, input variables, and output variables, as explained in Bianconi et al. (2010).

Table 1 Experimental test data

Source	Specimen	D (mm)	t (mm)	f_c (MPa)	E_c (MPa)	f_y (MPa)	E_s (MPa)	L (mm)	ξ	D/t	L/D	P_u (kN)
Gardener and Jacobson (Gardener & Jacobson, 1967; Gardener, 1968)	C-SPECIMEN8	120.8	4.06	34.40	27,566	452	191,536	241.3	1.962	30	2.0	1201
	C-SPECIMEN9	120.8	4.09	29.58	25,562	452	191,536	241.4	2.300	30	2.0	1201
	C-SPECIMEN10	120.8	4.09	25.92	23,928	452	191,536	241.4	2.625	30	2.0	1112
	C-SPECIMEN13	152.6	3.18	20.89	21,482	415	203,395	304.8	1.766	48	2.0	1201
	C-SPECIMEN14	152.6	3.15	23.10	22,589	415	203,395	304.8	1.581	48	2.0	1201
	C-SPECIMEN4	101.7	3.07	31.16	26,236	605	207,050	203.3	2.575	33	2.0	1068
	C-SPECIMEN3	101.7	3.07	34.13	27,458	605	207,050	203.3	2.351	33	2.0	1112
	C-SPECIMEN3a	169.3	2.62	36.54	28,411	317	195,811	305	0.563	65	1.8	1307
Tomii et al. (1977)	C-4HN	150	4.3	28.71	25,183	280	209,720	450	1.222	35	3.0	1203
	C-4HN	150	4.3	28.71	25,183	280	209,720	450	1.222	35	3.0	1225
	C-4HN	150	4.3	28.71	25,183	280	209,720	450	1.222	35	3.0	1200
	C-3HN	150	3.2	28.71	25,183	287	190,120	450	0.911	47	3.0	1040
	C-3HN	150	3.2	28.71	25,183	287	190,120	450	0.911	47	3.0	998
	C-3HN	150	3.2	28.71	25,183	287	190,120	450	0.911	47	3.0	980
	C-2HN	150	2	28.71	25,183	336	211,680	450	0.65	75	3.0	882
	C-2HN	150	2	28.71	25,183	336	211,680	450	0.65	75	3.0	882
	C-4MN	150	4.3	21.95	22,020	280	209,720	450	1.599	35	3.0	1065
	C-4MN	150	4.3	21.95	22,020	280	209,720	450	1.599	35	3.0	1087
	C-4MN	150	4.3	21.95	22,020	280	209,720	450	1.599	35	3.0	1096
	C-3MN	150	3.2	21.95	22,020	287	190,120	450	1.191	47	3.0	841
	C-3MN	150	3.2	21.95	22,020	287	190,120	450	1.191	47	3.0	840
	C-3MN	150	3.2	21.95	22,020	287	190,120	450	1.191	47	3.0	858
	C-2MN	150	2	21.95	22,020	336	211,680	450	0.85	75	3.0	773
	C-2MN	150	2	21.95	22,020	336	211,680	450	0.85	75	3.0	756
	C-4LN	150	4.3	18.03	19,957	280	209,720	450	1.946	35	3.0	963
	C-3LN	150	3.2	18.03	19,957	287	190,120	450	1.45	47	3.0	790
	C-3LN	150	3.2	18.03	19,957	287	190,120	450	1.45	47	3.0	790
	C-3LN	150	3.2	18.03	19,957	287	190,120	450	1.45	47	3.0	747
	C-2LN	150	2	18.03	19,957	336	211,680	450	1.035	75	3.0	656
	C-2LN	150	2	18.03	19,957	336	211,680	450	1.035	75	3.0	638
	C-2LN	150	2	18.03	19,957	336	211,680	450	1.035	75	3.0	672
Sakino and Hayashi (1991)	C-L-20–1	178	9	22.15	22,120	283	200,000	360	3.036	20	2.0	2042
	C-L-20–2	178	9	22.15	22,120	283	200,000	360	3.036	20	2.0	2102
	C-H-20–1	178	9	45.37	31,658	283	200,000	360	1.482	20	2.0	2667
	C-H-20–2	178	9	45.37	31,658	283	200,000	360	1.482	20	2.0	2677
	C-L-32–1	179	5.5	22.15	22,120	248	200,000	360	1.514	33	2.0	1467
	C-L-32–2	179	5.5	23.91	22,982	248	200,000	360	1.403	33	2.0	1530
	C-H-32–1	179	5.5	43.61	31,038	248	200,000	360	0.769	33	2.0	2040
	C-H-32–2	179	5.5	43.61	31,038	248	200,000	360	0.769	33	2.0	2030
	C-L-58–1	174	3	23.91	22,982	266	200,000	360	0.809	58	2.1	1135
	C-L-58–2	174	3	23.91	22,982	266	200,000	360	0.809	58	2.1	1135
	C-H-58–1	174	3	45.67	31,762	266	200,000	360	0.423	58	2.1	1608
	C-H-58–2	174	3	45.67	31,762	266	200,000	360	0.423	58	2.1	1677
Source	Specimen	D (mm)	t (mm)	f_c (MPa)	E_c (MPa)	f_y (MPa)	E_s (MPa)	L (mm)	ξ	D/t	L/D	P_u (kN)
O'Shea and Bridge (1994, 1998)	NC-R12CF1	190	1.15	110.3	32,405	202	193,200	662	0.045	165	3.5	2991
	NC-R12CF3	190	1.15	110.3	32,405	202	193,200	662	0.045	165	3.5	3137

Table 1 (continued)

Source	Specimen	D (mm)	t (mm)	f_c (MPa)	E_c (MPa)	f_y (MPa)	E_s (MPa)	L (mm)	ξ	D/t	L/D	P_u (kN)
	C-S10CS50A	190	0.86	41	17,810	211	177,000	659	0.094	221	3.5	1350
	NC-S12CS50A	190	1.13	41	17,810	186	178,400	664.5	0.11	168	3.5	1377
	NC-S16CS50B	190	1.52	48.3	21,210	306	207,400	664.5	0.208	125	3.5	1695
	S-S20CS50A	190	1.94	41	17,810	256	204,700	663.5	0.263	98	3.5	1678
	C-S30CS50B	165	2.82	48.3	21,210	363	200,600	580.5	0.541	59	3.5	1662
	S-S10CS80B	190	0.86	74.7	27,576	211	177,000	663.5	0.052	221	3.5	2451
	NC-S12CS80A	190	1.13	80.2	28,445	186	178,400	662.5	0.056	168	3.5	2295
	NC-S16CS80A	190	1.52	80.2	28,445	306	207,400	663.5	0.125	125	3.5	2602
	C-S20CS80B	190	1.94	74.7	27,576	256	204,700	663.5	0.144	98	3.5	2592
	C-S30CS80A	165	2.82	80.2	28,445	363	200,600	580.5	0.326	59	3.5	2295
Schneider (1998)	C-C1	140.8	3	28.18	25,599	285	189,475	602	0.92	47	4.3	790
	C-C2	141.4	6.5	23.81	23,528	313	206,011	602	2.797	22	4.3	1332
Tan et al. (1999)	C-A1-1	125	1	106	48,389	232	200,000	438	0.072	125	3.5	1275
	C-A1-2	125	1	106	48,389	232	200,000	438	0.072	125	3.5	1239
	C-A2-1	127	2	106	48,389	258	200,000	445	0.161	64	3.5	1491
	C-A2-2	127	2	106	48,389	258	200,000	445	0.161	64	3.5	1339
	C-A3-1	133	3.5	106	48,389	352	200,000	465	0.379	38	3.5	1995
	C-A3-2	133	3.5	106	48,389	352	200,000	465	0.379	38	3.5	1991
	C-A4-1	133	4.7	106	48,389	352	200,000	465	0.524	28	3.5	2273
	C-A4-2	133	4.7	106	48,389	352	200,000	465	0.524	28	3.5	2158
	C–C-1	133	4.7	92	45,081	352	200,000	465	0.604	28	3.5	1854
	C–C-2	133	4.7	92	45,081	352	200,000	465	0.604	28	3.5	1933
	C-B-3	108	4.5	96	46,050	358	200,000	379	0.709	24	3.5	1518
Yamamoto et al. (2000)	C-C10A-2A-3	101.8	3.03	23.2	22,638	371	200,000	305	2.088	34	3.0	628
	C-C20A-2A	216.4	6.61	24.3	23,169	452	200,000	650	2.499	33	3.0	3278
	C-C30A-2A	318.3	10.36	24.2	23,121	335	200,000	950	1.995	31	3.0	6319
	C-C20A-4A	216.4	6.61	46.8	32,153	452	200,000	650	1.298	33	3.0	4214
	C-C10A-4A-1	101.9	3.03	51.3	33,663	371	200,000	305	0.943	34	3.0	877
	C-C30A-4A	318.5	10.36	52.2	33,957	334	200,000	950	0.921	31	3.0	8289
Huang et al. (2002)	C-CU-040	200	5	27.15	24,490	266	200,000	600	1.058	40	3.0	1951
	C-CU-070	280	4	31.15	26,232	273	200,000	840	0.523	70	3.0	3025
	S-CU-150	300	2	27.23	24,526	342	200,000	900	0.342	150	3.0	2608
Han and Yao (2004)	C-scv2-1	200	3	49.5	37,420	304	206,500	600	0.386	67	3.0	2383
	C-scv2-2	200	3	49.5	37,420	304	206,500	600	0.386	67	3.0	2256
Giakomelis and Lam (2004)	C-C7	114.9	4.91	28.23	24,972	365	200,000	300.5	2.53	23	2.6	1020
	C-C9	115	5.02	48.6	32,765	365	200,000	300.5	1.506	23	2.6	1378
	C-C11	114.3	3.75	48.6	32,765	343	200,000	300	1.026	30	2.6	1033
	C-C12	114.3	3.85	25.71	23,831	343	200,000	300	1.997	30	2.6	761
	C-C4	114.6	3.99	83.6	42,974	343	200,000	300	0.637	29	2.6	1308
	C-C8	115	4.92	94.9	45,786	365	200,000	300	0.753	23	2.6	1787
	C-C14	114.5	3.84	88.9	44,315	343	200,000	300	0.575	30	2.6	1359

Source	Specimen	D (mm)	t (mm)	f_c (MPa)	E_c (MPa)	f_y (MPa)	E_s (MPa)	L (mm)	ξ	D/t	L/D	P_u (kN)
Sakino et al. (2004)	C-CC4-A-4–1	149	2.96	40.5	29,911	308	200,000	447	0.642	50	3.0	1064
	C-CC8-A-8	108	6.47	77	41,242	853	200,000	324	3.221	17	3.0	2667
	C-CC8-C-8	222	6.47	77	41,242	843	200,000	666	1.397	34	3.0	7304
	S-CC8-D-8	337	6.47	85.1	43,357	823	200,000	1011	0.788	52	3.0	13,776
	S-CC4-D-4–1	450	2.96	41.1	30,131	279	200,000	1350	0.182	152	3.0	6870

Table 1 (continued)

Source	Specimen	D (mm)	t (mm)	f_c (MPa)	E_c (MPa)	f_y (MPa)	E_s (MPa)	L (mm)	ξ	D/t	L/D	P_u (kN)
	S-CC4-D-4–2	450	3	41	30,131	279	200,000	1350	0.182	152	3.0	6985
Han et al. (2005)	C-CA1-1	60	1.87	75.2	41,540	282	201,500	180	0.515	32	3.0	312
	C-CA1-2	60	1.87	75.2	41,540	282	201,500	180	0.515	32	3.0	320
	C-CA2-1	100	1.87	75.2	41,540	282	201,500	300	0.297	53	3.0	822
	C-CA2-2	100	1.87	75.2	41,540	282	201,500	300	0.297	53	3.0	845
	C-CA3-1	150	1.87	75.2	41,540	282	201,500	450	0.194	80	3.0	1701
	C-CA3-2	150	1.87	75.2	41,540	282	201,500	450	0.194	80	3.0	1670
	C-CA4-1	200	1.87	75.2	41,540	282	201,500	600	0.144	107	3.0	2783
	C-CA4-2	200	1.87	75.2	41,540	282	201,500	600	0.144	107	3.0	2824
	NC-CA5-1	250	1.87	75.2	41,540	282	201,500	750	0.115	134	3.0	3950
	NC-CA5-2	250	1.87	75.2	41,540	282	201,500	750	0.115	134	3.0	4102
	C-CB2-1	100	2	75.2	41,540	404	207,000	300	0.457	50	3.0	930
	C-CB2-2	100	2	75.2	41,540	404	207,000	300	0.457	50	3.0	920
	C-CB3-1	150	2	75.2	41,540	404	207,000	450	0.298	75	3.0	1870
	C-CB3-2	150	2	75.2	41,540	404	207,000	450	0.298	75	3.0	1743
	S-CB4-1	200	2	75.2	41,540	404	207,000	600	0.222	100	3.0	3020
	S-CB4-2	200	2	75.2	41,540	404	207,000	600	0.222	100	3.0	3011
	S-CB5-1	250	2	75.2	41,540	404	207,000	750	0.176	125	3.0	4442
	S-CB5-2	250	2	75.2	41,540	404	207,000	750	0.176	125	3.0	4550
	C-CC2-1	150	2	80	41,540	404	207,000	450	0.281	75	3.0	1980
	C-CC2-2	150	2	80	41,540	404	207,000	450	0.281	75	3.0	1910
	S-CC3-1	250	2	80	41,540	404	207,000	750	0.166	125	3.0	4720
	S-CC3-2	250	2	80	41,540	404	207,000	750	0.166	125	3.0	4800
Gupta et al. (2007)	C-D3M4C2	89.32	2.74	33	26,999	360	200,000	340	1.473	33	3.8	494
	C-D3M4F13	89.32	2.74	31.48	26,370	360	200,000	340	1.544	33	3.8	495
	C-D3M4F22	89.32	2.74	31.48	26,370	360	200,000	340	1.544	33	3.8	478
	C-D3M4F33	89.32	2.74	28.19	24,954	360	200,000	340	1.724	33	3.8	529
	C-D4M4C1	112.6	2.89	30.84	26,101	360	200,000	340	1.297	39	3.0	702
	C-D4M4F13	112.6	2.89	31.48	26,370	360	200,000	340	1.271	39	3.0	757
	C-D4M4F21	112.6	2.89	25.28	23,631	360	200,000	340	1.583	39	3.0	659
	C-D4M4F32	112.6	2.89	26.2	24,057	360	200,000	340	1.527	39	3.0	638
Yu et al. (2007)	C-SZ3S4A1	165	2.72	48	32,563	350	213,000	510	0.506	61	3.1	1750
	C-SZ3S6A1	165	2.73	67.2	38,529	350	213,000	510	0.363	60	3.1	2080
de Oliveira (2009)	C–C-30-3D	114.3	3.35	32.7	26,876	287	206,000	342.9	1.128	34	3.0	669
	C–C-60-3D	114.3	3.35	58.7	36,009	287	206,000	342.9	0.629	34	3.0	946
	C–C-80-3D	114.3	3.35	88.8	44,290	287	206,000	342.9	0.416	34	3.0	1133
	C–C-100-3D	114.3	3.35	105.5	48,275	287	206,000	342.9	0.350	34	3.0	1455
Source	Specimen	D (mm)	t (mm)	f_c (MPa)	E_c (MPa)	f_y (MPa)	E_s (MPa)	L (mm)	ξ	D/t	L/D	P_u (kN)
Lee et al. (2011)	C-049C36 30	360	6	31.5	26,379	498	202,000	1760	1.109	60	4.9	6888
Xiong et al. (2017)	C-C3	114.3	3.6	173.5	63,000	403	213,000	250	0.323	32	2.2	2422
	C-C4	114.3	3.6	173.5	63,000	403	213,000	250	0.323	32	2.2	2340
	C-C5	114.3	3.6	184.2	63,000	403	213,000	250	0.304	32	2.2	2497
	C-C6	114.3	3.6	184.2	63,000	403	213,000	250	0.304	32	2.2	2314
	C-C7	114.3	6.3	173.5	63,000	428	209,000	250	0.649	18	2.2	2610
	C-C8	114.3	6.3	173.5	63,000	428	209,000	250	0.649	18	2.2	2633
	C-C9	219.1	5	51.6	28,000	377	205,000	600	0.684	44	2.7	3118
	C-C10	219.1	5	185.1	66,000	377	205,000	600	0.199	44	2.7	7813

Table 1 (continued)

Source	Specimen	D (mm)	t (mm)	f_c (MPa)	E_c (MPa)	f_y (MPa)	E_s (MPa)	L (mm)	ξ	D/t	L/D	P_u (kN)
	C-C11	219.1	5	193.3	66,000	377	205,000	600	0.191	44	2.7	8527
	C-C12	219.1	10	51.6	28,000	381	212,000	600	1.489	22	2.7	4309
	C-C13	219.1	10	185	66,000	381	212,000	600	0.435	22	2.7	9085
	C-C14	219.1	10	193.3	66,000	381	212,000	600	0.416	22	2.7	9187
	C-C15	219.1	6.3	163	66,000	300	202,000	600	0.231	35	2.7	6915
	C-C16	219.1	6.3	175.4	59,000	300	202,000	600	0.215	35	2.7	7407
	C-C17	219.1	6.3	148.8	52,000	300	202,000	600	0.254	35	2.7	6838
	C-C18	219.1	6.3	174.5	52,000	300	202,000	600	0.216	35	2.7	7569
Guler et al., (2013, 2014)	C-CF3-1	76.19	2.99	145	56,595	278	200,000	300	0.341	25	3.9	795
	C-CF3.3–1	76.18	3.31	145	56,595	305	200,000	300	0.419	23	3.9	847
	C-C4NG-1	114.2	4.02	115	50,402	306	200,000	400	0.418	28	3.5	1428
	C-C6NG-1	114.3	5.98	115	50,402	314	200,000	400	0.675	19	3.5	1833
Han et al. (2014)	C-c0	160	3.83	51	33,900	409	200,000	480	0.827	42	3.0	2023

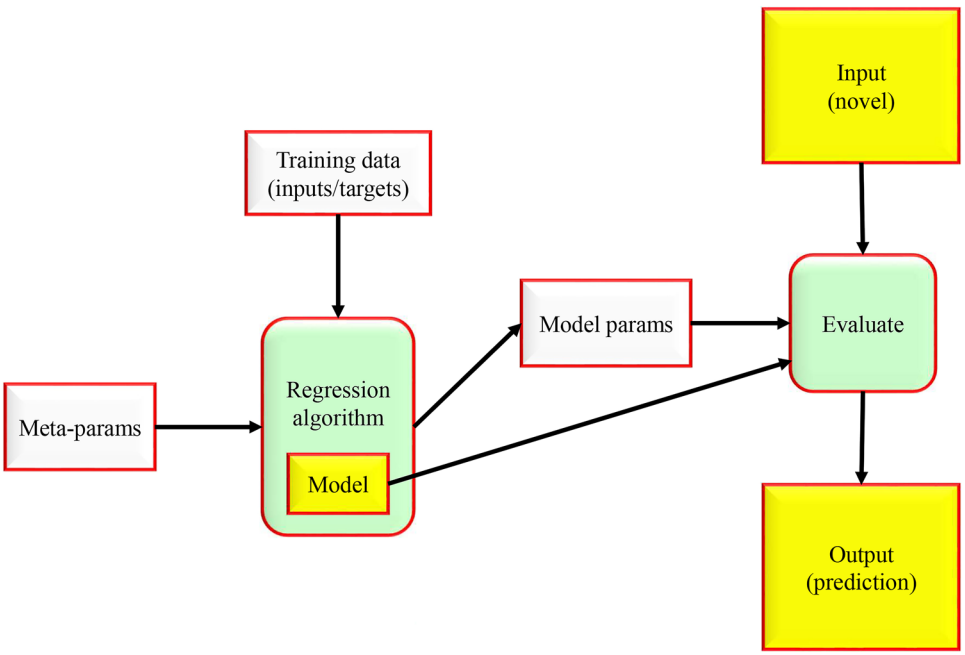

Fig. 2 Typical flowchart for regression

Backpropagation neural networks are employed in this study due to its high capability of data mapping (Hecht-Nielsen, 1989). Backpropagation learning is primarily based on the gradient descent along the error surface (Gallant, 1987; Haykin, 1998; Kamarthi & Pittner, 1999). The weight adjustment is proportional to the negative gradient of the error to the weight. The mathematical representation is given by Eq. (1):

$$w_{k+1} = w_k + \eta \mathrm{d}_k \tag{1}$$

where, w_k = an individual weight at epoch k, η = the learning rate, and the direction vector d_k is negative of the gradient of the output error function $\varepsilon E\varepsilon$ as stated below in Eq. (2):

$$d_k = -\nabla E(w_k) \tag{2}$$

3.2 Transfer Function

There exist five types of transform functions, including the linear function, threshold function, sigmoid function,

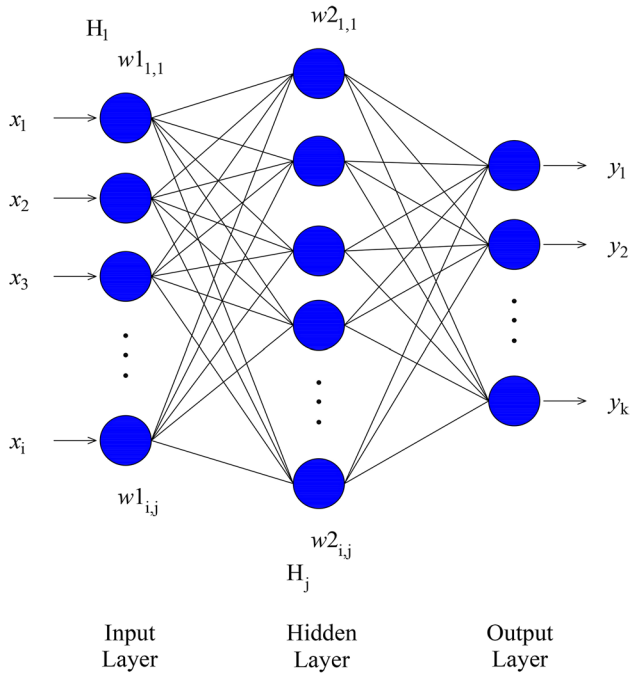

Fig. 3 Typical feedforward network (FFN) model

hyperbolic tangent function, and radial basis function to transform the input signal into output (Roshan, 2007). In this paper, the sigmoid transfer functions are used. The *log* and *tan* sigmoidal functions were used for squashing the weights between the layers (Fig. 4). To build a neural network that performs some definite task, one chooses how the units are connected to another and sets the weights on the connections appropriately. The connections conclude whether it is possible that one unit to influence another. The weights specify the strength of the influence.

3.3 Error Backpropagation Algorithm

Error backpropagation (EBP) algorithm is the most popular and can be used for neural network training. The rule for this algorithm is represented in Eq. (3):

$$\Delta w_k = -\alpha g_k \tag{3}$$

where, w and g, as stated above, can be calculated using the following equations:

$$g = \left[\frac{\partial E}{w_1}, \frac{\partial E}{w_2}, \frac{\partial E}{w_3}\right] \tag{4}$$

$$w = \left[w_1, w_2, w_3 \cdots\right] \tag{5}$$

This algorithm has been developed based on gradient optimization. Although it is easy and stable in the training process, it became unpopular due to its limited power and slow convergence.

3.4 Newton Algorithm

Newton algorithm, is also known as the gradient descent algorithm, using the derivative of a gradient to evaluate the change of the gradient, then selects proper learning constants in each direction (Osborne, 1992). The rule for this algorithm is computed by the following equation.

$$\Delta w_k = -H_k^{-1} g_k \tag{6}$$

where, g and H are defined as follows:

$$g_i = \frac{\partial E}{\partial w_i} \tag{7}$$

Fig. 4 Transfer functions

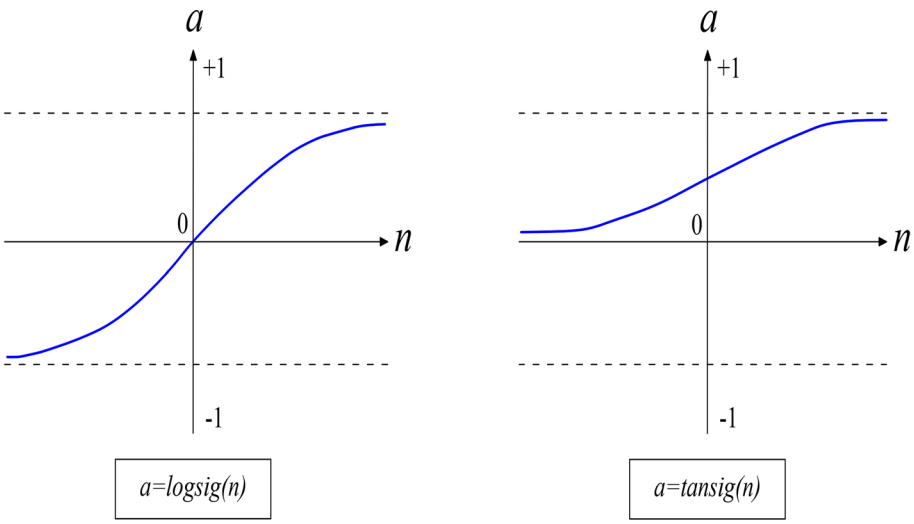

$$H = \begin{bmatrix} \frac{\partial^2 E}{\partial w_1^2} & \frac{\partial^2 E}{\partial w_1 \partial w_2} & \cdots & \frac{\partial^2 E}{\partial w_1 \partial w_N} \\ \frac{\partial^2 E}{\partial w_2 \partial w_1} & \frac{\partial^2 E}{\partial w_2^2} & \cdots & \frac{\partial^2 E}{\partial w_2 \partial w_N} \\ \cdots & \cdots & \cdots & \cdots \\ \frac{\partial^2 E}{\partial w_N \partial w_1} & \frac{\partial^2 E}{\partial w_N \partial w_2} & \cdots & \frac{\partial^2 E}{\partial w_N^2} \end{bmatrix} \tag{8}$$

The mathematical formula for computing E is shown in Eq. (9). This algorithm has a faster convergence than the EBP algorithm. However, the training process is unstable and, computing second-order derivatives is time-consuming. Due to these drawbacks, this algorithm became unpopular.

$$E = \frac{1}{2} \sum_{p=1}^{P} \sum_{m=1}^{M} e_{\mathrm{pm}}^2 \tag{9}$$

3.5 Gauss–Newton Algorithm

This algorithm has a slight modification of Newton algorithm, i.e., the elimination of the second-order derivatives in the Newton method was done by introducing the Jacobian matrix (J). This algorithm has faster convergence; however, the stability in the training process is negative, and for this reason, a newer algorithm is required. This algorithm is stated using the following equation:

$$\Delta w_k = -\left(J_k^T J_k^{-1} J_k^T e_k\right) \tag{10}$$

where, g and H are defined as follows:

$$g = J^T e \tag{11}$$

$$H \approx J^T J \tag{12}$$

Here J, and e can be written as follows:

$$J = \begin{bmatrix} \frac{\partial e_{1,1}}{\partial w_1} & \frac{\partial e_{1,1}}{\partial w_2} & \cdots & \frac{\partial e_{1,1}}{\partial w_N} \\ \frac{\partial e_{1,2}}{\partial w_1} & \frac{\partial e_{1,2}}{\partial w_2} & \cdots & \frac{\partial e_{1,2}}{\partial w_N} \\ \cdots & \cdots & \cdots & \cdots \\ \frac{\partial e_{1,M}}{\partial w_1} & \frac{\partial e_{1,M}}{\partial w_2} & \cdots & \frac{\partial e_{1,M}}{\partial w_N} \\ \cdots & \cdots & \cdots & \cdots \\ \frac{\partial e_{P,1}}{\partial w_1} & \frac{\partial e_{P,1}}{\partial w_2} & \cdots & \frac{\partial e_{P,1}}{\partial w_N} \\ \frac{\partial e_{P,2}}{\partial w_1} & \frac{\partial e_{P,2}}{\partial w_2} & \cdots & \frac{\partial e_{P,2}}{\partial w_N} \\ \cdots & \cdots & \cdots & \cdots \\ \frac{\partial e_{P,M}}{\partial w_1} & \frac{\partial e_{P,M}}{\partial w_2} & \cdots & \frac{\partial e_{P,M}}{\partial w_N} \end{bmatrix} \tag{13}$$

$$e = \begin{bmatrix} e_{1,1} \\ e_{1,2} \\ \cdots \\ e_{1,M} \\ \cdots \\ e_{P,1} \\ e_{P,2} \\ \cdots \\ e_{P,M} \end{bmatrix} \tag{14}$$

3.6 Levenberg Marquardt algorithm

Levenberg–Marquardt (LM) algorithm is an iterative technique that identify the minimum of a multivariate function, which is expressed as the sum of squares of nonlinear real-valued functions (Levenberg, 1944; Marquardt, 1963). This technique was found to have diversified applications (Mittelmann, 2004). This technique is evolved as a combination of steepest descent and the Gauss–Newton method. When the current solution is far from the correct ones, the algorithm behaves like a steepest descent method: slow but guaranteed convergence to 1. When the current solution is near the correct solution, it becomes a Gauss–Newton method. Here, a short explanation of the LM algorithm based Madsen et al. (2004) is supplied. LM algorithm combines the features of the blend EBP algorithm and Gaussian-Newton algorithm, eventually, it can be determined using Eq. (15).

$$\Delta w_k = -\left(J_k^T J_k + \mu_k I\right)^{-1} J_k e_k \tag{15}$$

During evaluation, when error increases and μ increase, LM algorithm switches to EBP algorithm. However, when the evaluation error decreases and μ decreases, LM algorithm switches to Gaussian-Newton method. This algorithm has both fast convergence and stable training. Compared to all other algorithms, the LM algorithm is more powerful. Despite its more complex computation, it has better searchability. Notwithstanding that a detailed analysis of the EBP, Gaussian-Newton, and LM algorithms can be referred to Madsen et al. (2004) and Gavin (2013).

4 ANN-Based Modeling Process

The primary goal of this investigation is to employ ANN principles to develop a model to predict the load capacity of circular CFSTCs. The general-purpose MATLAB® R2016a software is used to develop an ANN-based model and discussed in more detail.

4.1 Input and Output

One hundred fifty datasets obtained from the results of the axial test on CFSTCs were used in the ANN-based model. The ultimate load capacity of CFSTCs, P_u, depends on several parameters given in Table 1 such as f_c, E_c, f_y, E_s, ξ, D/t, and L/D, and these parameters were considered input terminals in the input layer for the ANN model, while P_u is the ANN's output.

4.2 Architecture on ANN

In this research, backpropagation ANN architecture has been employed, which contains four layers, i.e., one input layer, two hidden layers, and one output layer. The transfer function '*tansig*' was considered between the input and first hidden layers; '*logsig*' was considered between the first hidden layer and the second hidden layer; '*logsig*' was further used between the second hidden layer and output layer. The transfer functions and the number of nodes in all layers remain the same for all models. The transfer functions used in MATLAB® for *tan* and *log* sigmoidal functions is shown in Eqs. (16), and (17), separately (Beale et al., 2010; Demuth et al., 2006).

$$tansig(n) = 2/(1 + \exp(-2 * n)) - 1 \tag{16}$$

$$logsig(n) = 1/(1 + \exp(-n)) \tag{17}$$

4.3 Training of ANN

About 75% of the total data sets are used to the ANN for training, while the remaining datasets are used to validate the developed model. The architecture of ANN is described in Fig. 5. The data that form an input vector (indicated in Table 1) have different quantitative limits. For this reason, data normalization (between 0 and 1) was done using Eq. (18) before developing the ANN-based model.

$$x_i^n = \frac{x_i^a - x_i^{min}}{x_i^{max} - x_i^{min}} \tag{18}$$

where, x_i^a and x_i^n i^{th} component of the input vector before and after normalization, respectively. x_i^{max} and x_i^{min} are the maximum and minimum values of the components of the input vector before normalization. The training phase of ANN converged at about 1000 iterations or epochs for P_u (see Fig. 6). To check the accuracy of a neural network structure, accordingly, to evaluate correlations of training data and testing data, the "Mean Squared Error" (MSE) criterion was considered in this study.

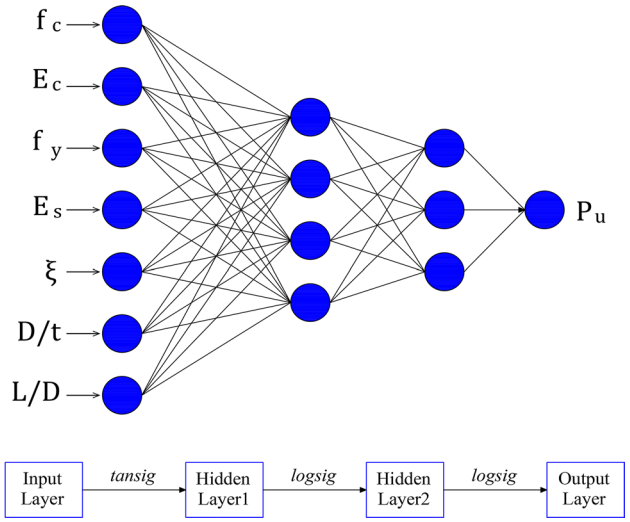

Fig. 5 Typical architecture of ANN

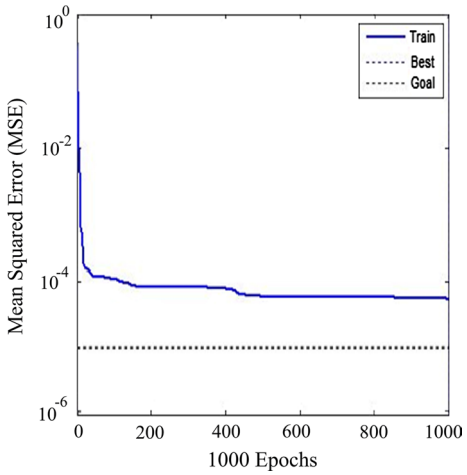

Fig. 6 Training performance for *Pu*

4.4 Testing of ANN

After the development of the ANN model, the model was verified with the remaining 25% dataset. The findings were listed and compared in Table 2. The ultimate load capacity predictions through the developed ANN model in the forms of time variation and scatter plot are illustrated in Fig. 7. The output vector obtained from the ANN model was normalized, in doing so, the normalized data were reverted to its actual value by using Eq. (19) as given as follows:

$$x_i^a = x_i^n\left(x_i^{max} - x_i^{min}\right) + x_i^{min} \tag{19}$$

Table 2 Comparison of experimental values with predicted results

f_c (MPa)	f_y (MPa)	ξ	D/t	L/D	$P_u^E(kN)$	$P_u^{ANN}(kN)$	P_u^{ANN}/P_u^E
25.92	452	2.625	30	2.0	1112	1054	0.95
23.10	415	1.581	48	2.0	1201	1124	0.94
34.13	605	2.351	33	2.0	1112	1027	0.92
28.71	287	0.911	47	3.0	1040	1002	0.96
28.71	287	0.911	47	3.0	998	965	0.97
21.95	280	1.599	35	3.0	1087	1003	0.92
21.95	280	1.599	35	3.0	1096	1021	0.93
21.95	287	1.191	47	3.0	840	865	1.03
18.03	280	1.946	35	3.0	963	975	1.01
18.03	287	1.45	47	3.0	790	821	1.04
18.03	287	1.45	47	3.0	747	732	0.98
18.03	336	1.035	75	3.0	672	632	0.94
22.15	283	3.036	20	2.0	2102	2043	0.97
45.37	283	1.482	20	2.0	2667	2543	0.95
23.91	248	1.403	33	2.0	1530	1598	1.04
43.61	248	0.769	33	2.0	2030	2078	1.02
45.67	266	0.423	58	2.1	1608	1654	1.03
110.3	202	0.045	165	3.5	2991	2876	0.96
48.3	306	0.208	125	3.5	1695	1604	0.95
74.7	211	0.052	221	3.5	2451	2376	0.97
80.2	186	0.056	168	3.5	2295	2204	0.96
28.18	285	0.92	47	4.3	790	732	0.93
23.2	371	2.088	34	3.0	628	639	1.02
24.3	452	2.499	33	3.0	3278	3365	1.03
24.2	335	1.995	31	3.0	6319	6421	1.02
77	843	1.397	34	3.0	7304	7120	0.97
85.1	823	0.788	52	3.0	13,776	13,432	0.98
41.1	279	0.182	152	3.0	6870	6643	0.97
75.2	282	0.515	32	3.0	320	301	0.94
75.2	282	0.115	134	3.0	4102	3987	0.97
80	404	0.166	125	3.0	4800	4621	0.96

where, x_i^n is the normalized result obtained after the test for the i^{th} component and x_i^a is the real results obtained for the i^{th} component, respectively. As can be observed in Table 2 and Fig. 7, the experimental ultimate load-bearing capacity values, P_u, and predicted values by the ANN-based model, P_u^{ANN}, are in excellent agreement. Figure 7 is a regression plot where network target (experimental axial load capacities) and output (predicted axial load capacities) data are plotted for each data point, as x and y coordinates, respectively. The variation between the predicted and the corresponding experimental values is found to be ±10%; hence, the developed ANN model is robust and reliable. The developed model was assessed using prominent engineering indices. For example, the coefficient of determination R-squared (R^2) is a statistical measure of how close the data are to the fitted regression line and assign values between 0 and 100%. 0% proves that none of the variability of the response data predicted by the model is around its mean, while 100% means that the variability of the response data is around its mean. The higher R^2 means the better model fitting the data. In the present study, the ANN-based model with R^2 of 0.9993 is a higher performance capacity for prediction, indicating that the fitted regression of the predicted value is closer to the experimental data. Further, a new engineering index, $a20-index$, has been proposed by Asteris and Mokos (2019) to verify the reliability of developing an ANN-based model. The final rank of the model was calculated by summing the ranking values for both training and testing stages (Eq. (20)).

$$a20-index=\frac{m20}{N} \tag{20}$$

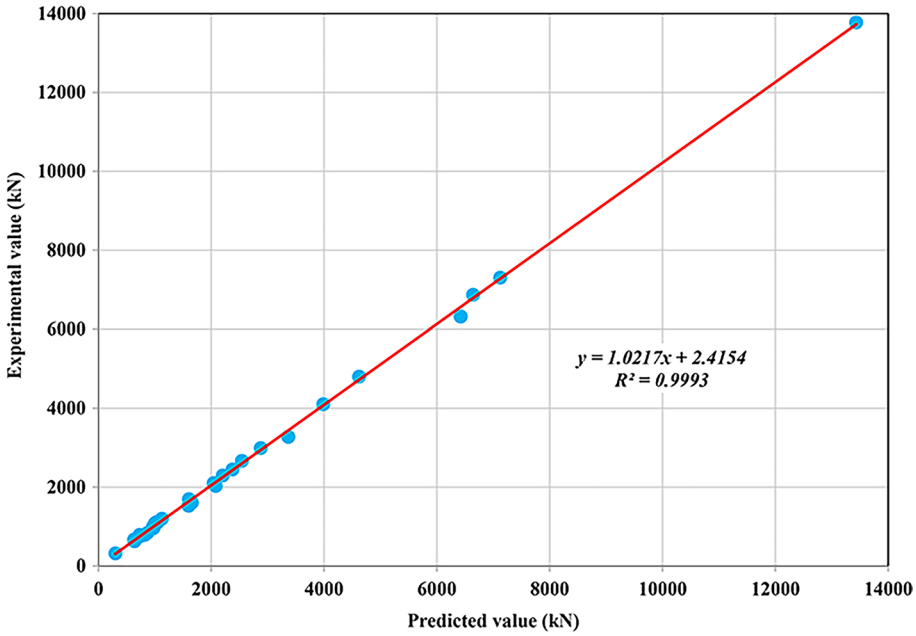

Fig. 7 Performance of testing set

where, N = No. of dataset sample, $m20$ = No. of samples whose value of the ratio experimental to estimated lies between 0.8 and 1.2. For the best model, $a20-index$ should be 1. The proposed a20-index has the advantage that its value has a physical engineering meaning. It represents the number of samples that predict values with a deviation of ±20% compared. In this paper, $a20-index$, for the case of training data set is 0.9832, and for validation, it is 0.9521. It shows the number of samples that the predicted values with a margin of ±20% against experimental observations.

5 Estimation of Load Capacity of Circular CFSTCs Using Various Analytical Models

Various models were conducted in the prior investigations considering the techniques for developing some statistical models to predict the ultimate axial load capacity of circular CFSTCs. For example, employing MARS and RVM modeling concepts to predict the ultimate load capacity of CFSTCs are reported in Avci-Karatas (2019, 2021). The author has proposed expressions to predict the same using soft computing methods of MARS and RVM-based models regarding modeling' applicability and capability. The input parameters of ANN developed here, to obtain the possibility of obtaining a stronger model, were the same parameters of data used previously in developing the MARS, and RVM-based models. Accordingly, the analytical conclusions of the ANN-based, the MARS-based, and the RVM-based models were briefly compared. The minimum and maximum values for the ratio of predicted and the experimental ultimate load in the ANN-based model, P_u^{ANN}/P_u^E,

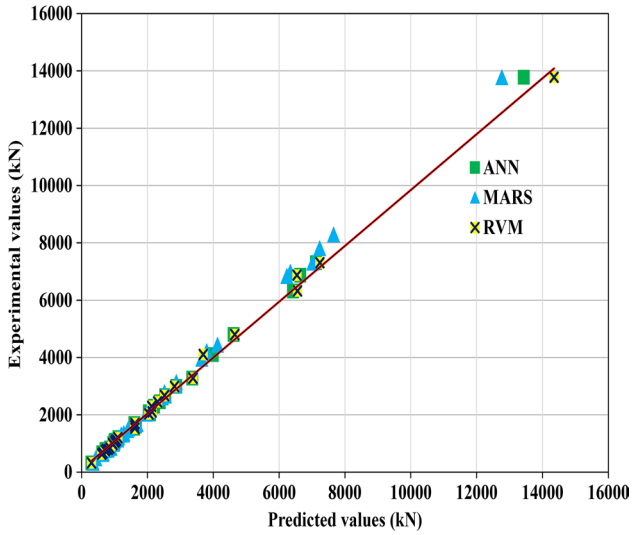

Fig. 8 Comparison of performance of ANN, MARS, and RVM-based models developed by Avci-Karatas (2019, 2021)

was found to vary in between 0.92 and 1.04 (see Table 2), while in the MARS-based model, P_u^{MARS}/P_u^E, varied in the range of 0.87 to 1.10, and P_u^{RVM}/P_u^E was found to vary between 0.90 and 1.06 in theRVM-based model. The findings presented in this paper showed that a satisfactory performance target, such as reduced convergence on the more scattering amplitudes of numerical results to the experimental ones, was performed by the newly developed ANN-based model for the considered data. A brief comparison of the above investigated models for the same data is given in Fig. 8. The detailed comparison of the experimental

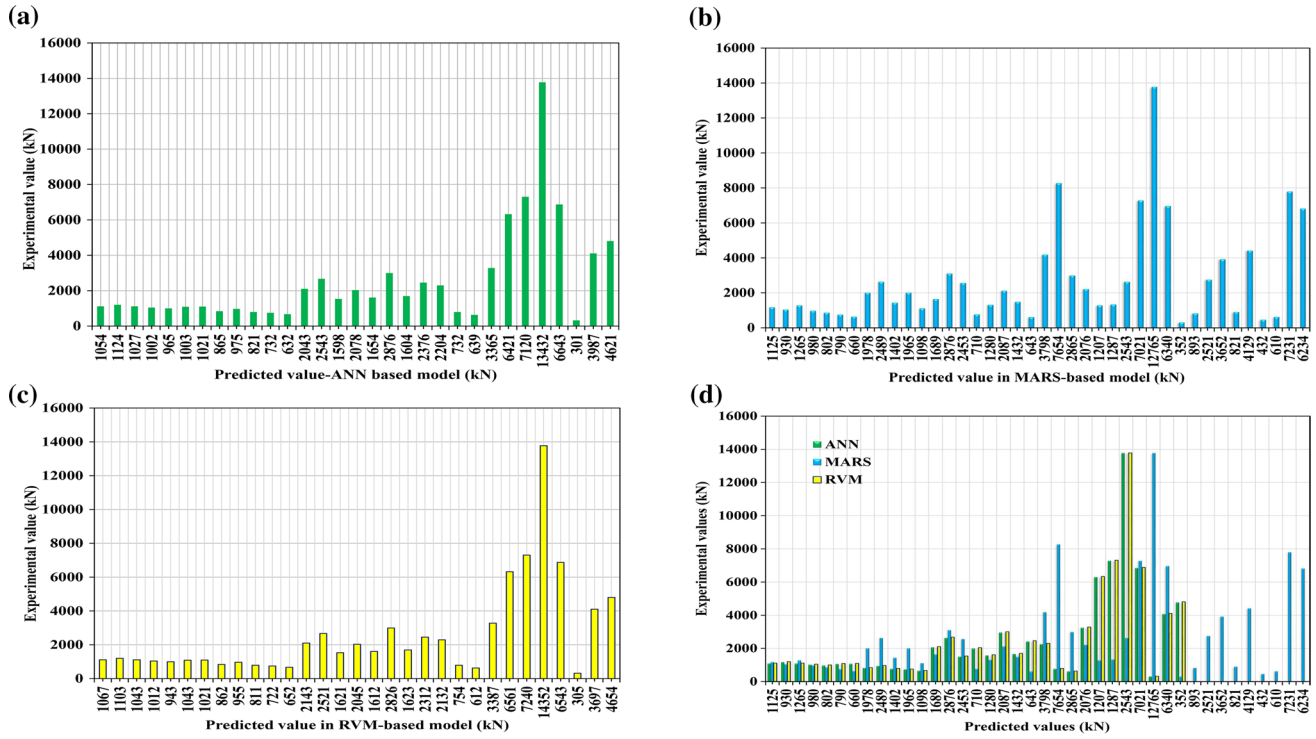

Fig. 9 Detailed comparison of the predicted results of analytical models with the experimental results: **a** ANN-based model; **b** MARS-based model; **c** RVM-based model; **d** a comparison of the combined performance of three analytical models newly here and previously developed by Avci-Karatas (2019, 2021)

values with the predictions of ANN, MARS and RVM are given in Fig. 9. Although, these two methods (i.e., MARS and RVM) are powerful soft-computing techniques, ANN reduces the running time substantially faster, regarding accuracy for the investigated scope in the present research. It can be explained that the ANN model yields preferable results than those of the MARS and RVM-based models to estimate the load capacity of circular CFSTCs. It can be said that there is an improved forecasting accuracy with ANN instead of MARS and RVM results based on the findings. Accordingly, this research verifies that if the order of preference for the best analytical modeling performance among these is made, it can be done in the form of ANN, RVM, and MARS-based modeling to estimate the ultimate load capacity of circular CFSTCs, respectively.

Meanwhile, the other codes of practice such as design specifications used to predict the load capacity of CFSTCs, i.e., ANSI/AISC 360−16, and EC4, are now considered in the context of this research. Table 3 shows the limitations of these design specifications:where K is the effective length factor based on column' end boundary conditions, λ refers the relative slenderness, δ is the ratio of steel contribution, and w_c is the concrete density in the range between 1500 and 2500kg/m^3.

Table 3 Design specification limitations for ANSI/AISC 360−16 and EC4

Parameters	ANSI/AISC 360−16	EC4
f_y(MPa)	$f_y \le 525$	$235 \le f_y \le 460$
f_c(MPa)	$21 \le f_c \le 70$	$20 \le f_c \le 60$
E_c	$0.043 w_c^{1.5} \sqrt{f_c}$	$22000(\frac{f_c+8}{10})^{0.3}$
D/t	$\le 0.31(\frac{E_s}{f_y})$	$\le 90(\frac{235}{f_y})$
Steel amount	$\ge 1\%$ of gross area	$0.2 \le \delta \le 0.9$
Slenderness	$KL/r \le 200$	$\lambda \le 2$

- ***ANSI/AISC 360-16***

  In the code of ANSI/AISC 360−16, which no big effect of ξ on its consideration, the CFSTC sections are classified as compact ($D/t < \lambda_p = 0.15E_s/f_y$), noncompact ($\lambda_p < D/t < \lambda_r = 0.19E_s/f_y$), or slender ($D/t > \lambda_r$). Furthermore, all for sections should be in the limitation of $D/t < 0.31E_s/f_y$). According to ANSI/AISC 360-16, the section types are classified in Table 1, and denoted by "C-" for compact, "NC-" for noncompact, and "S-" for slender as the prefix of specimen name. The nominal compressive strength of CFSTCs, P_u^{AISC}, shall be determined as follows:

$$P_u^{AISC} = P_{no}\left[0.658^{\frac{P_{no}}{P_e}}\right]\frac{P_{no}}{P_e} \le 2.25 \tag{21}$$

$$P_u^{AISC} = 0.877P_e\frac{P_{no}}{P_e} > 2.25 \tag{22}$$

where, P_{no} is the nominal strength of the composite section, and $P_e$is the Euler critical load. For compact section, P_{no} is calculated as:

$$P_{no} = P_p = A_s f_y + A_c \xi f_c \tag{23}$$

where, P_p is the plastic strength of the circular section, A_s and A_c are the cross-sectional areas of the steel tube, and the concrete, respectively. ANSI/AISC 360−16 adopts the confinement effect of a circular section as $\xi = 0.95$. For noncompact section, P_{no} is evaluated as:

$$P_{no} = P_p - \frac{P_p - \left(A_s f_y + 0.7A_c f_c\right)}{\left(\lambda_r - \lambda_p\right)^2}(\lambda - \lambda_p)^2 \tag{24}$$

For slender section, P_{no} is given by:

$$P_{no} = A_s\frac{0.72f_y}{(\left(\frac{D}{t}\right)\frac{f_y}{E_s})^{0.2}} + 0.7A_c f_c \tag{25}$$

- ***EC4***

In EC4, which takes the effect of ξ on its consideration, the plastic compressive capacity of circular CFSTCs, P_u^{EC4}, is calculated as follows:

$$P_u^{EC4} = \eta_a A_s f_y + A_c f_c\left(1 + \eta_c\frac{tf_y}{Df_c}\right) \tag{26}$$

where, η_a = the steel reduction factor, and η_c = the concrete enhancement factor can be obtained as:

$$\eta_a = 0.25(3 + 2\bar{\lambda}) \le 1.0 \tag{27}$$

$$\eta_c = 4.9 - 18.5\bar{\lambda}^2 \ge 0 \tag{28}$$

EC4 takes the ξ effect within its consideration that represents by the term $(1 + \eta_c\frac{tf_y}{Df_c})$ as shown in Eq. (26). $\bar{\lambda}$ is the relative slenderness ratio which is given by:

$$\bar{\lambda} = \sqrt{\frac{\left(A_s f_y + A_c f_c\right)}{\frac{(\pi^2(E_s I_s + K_e E_c I_c)}{(KL)^2}}} \le 0.5 \tag{29}$$

where, I_s, I_c are the moment of inertia of steel tube section and concrete section, respectively. The confinement effect is considered, if the value of does not exceed 0.5. The correction factor, $K_e = 0.6$. EC4 considered the effect of imperfections by a reduction factor χ:

$$\chi = \frac{1}{0.5\left[1 + \alpha\left(\bar{\lambda} - 2\right) + \bar{\lambda}^2\right] + (\left(0.5\left[1 + \alpha\left(\bar{\lambda} - 2\right) + \bar{\lambda}^2\right]\right)^2 - \bar{\lambda}^2)^{0.5}} \le 1.0 \tag{30}$$

The imperfection factor, $\alpha = 0.21$ for circular CFSTCs. The parameters of geometrical and material properties of specimens are the effect on the predictions of both codes with different percentages. The calculation methods defined in the specifications are used within certain limits. It can be found for the specifications that these design models underestimate the ultimate load capacity of circular CFSTCs. The performance of the proposed formula in this paper is valid within the limits of the dataset used also includes data beyond these limits regarding existing these specifications. As mentioned before, the effecting of key parameters for circular CFSTCs to the predicted load capacity for this research was considered, and verified by experimental ones.

6 Conclusions

In the present day design case scenarioa with the addition of experimental work, usage of appropriate software adds quality and enhances the validity of the work. In the present study, by employing the ANN modeling concept, an advanced statistical model has been developed to predict the ultimate capacity of circular CFSTC members under axial compression loadings. Large data on CFSTCs considering variations in the geometrical and mechanical properties have been collected and consolidated for developing a model. Key input variables have been identified for predicting the ultimate capacity of CFSTCs. For developing an ANN model, the backpropagation-training technique was employed for updating the weights of each layer based on the error in the network output. The ANN architecture consists of one input, one output, and two hidden layers. The sigmoidal transfer functions are used for squashing the weights between the layers. Levenberg–Marquardt algorithm was used for feed-forward-backpropagation. ANN model was developed using MATLAB® software for training and prediction of the ultimate load capacity of CFSTC. ANN has been trained with about 75% of the total datasets and tested with about 25% of the remaining data sets. The predicted ultimate capacity is compared with that of the corresponding experimental value and the percentage difference between the predicted values and the corresponding experimental values is found to be less than 10%. $R^2 = 0.9993$, meaning the developed model fits the data nearly perfectly. The ratio of predicted and the corresponding experimental ultimate load P_u^{ANN}/P_u^E

was found to vary between 0.92 and 1.04. It shows the strong modeling that the predicted and actual values of the axial load capacity are much closer. In this regard, the proposed ANN-based model was trained, verified, and evaluated by conducting the difference from the previous model and the new concluding remarks derived from the findings. An evaluation was made by comparing the performance of analytical models (i.e., MARS and RVM) improved by the author on the same data in the previous studies. In this regard, the design specifications for the circular CFSCTs described in ANSI/AISC 360−16, and EC4 were discussed to make verification on the considered input data, which affect the load capacity. As a result, the reliability of the newly developed model has been validated with a dataset comprising 150 experimental data results available in the literature. In this regard, the developed ANN-based model will serve as a beneficial tool for handling structural engineering problems of the design of circular CFSTCs in accordance with experimental investigations.

Funding No funding was received to assist with the preparation of this article.

Data Availability and Materials Some or all data, models, or code generated or used during the study are available from the corresponding author by request.

Declarations

Conflict of interest The author has no conflicts of interest to declare that are relevant to the content of this article.

References

Abdelkarim, O.I., Gheni, A., Anumolu, S., Wang, S., & Elgawady, M. (2015). *Hollow-core FRP-concrete-steel bridge columns under extreme loading*. Report No. cmr15-008, Missouri Department of Transportation Research, Development and Technology, Missouri University of Science and Technology.

AISC 360−16. (2016). ANSI/AISC 360−16 *Specification for Structural Steel Buildings* (pp. 676). Chicago, Illinois, USA. https://www.aisc.org/Specification-for-Structural-Steel-Buildings-ANSIAISC-360-16-1.

Akbas, B., Shen, J., & Sabol, T. A. (2011). Estimation of seismic-induced demands on column splices with a neural network model. *Applied Soft Computing, 11*(8), 4820–4829. https://doi.org/10.1016/j.asoc.2011.06.019

Al-eliwi, B., Ekmekyapar, T., & Al-juboori, H. A. (2017). Comparison of AISC 360–16 and EC4 for the prediction of composite column capacity. *The International Journal of Energy and Engineering Sciences (IJEES), 2*(2), 3–22.

Aslani, F., Uy, B., Tao, Z., & Mashiri, F. (2015). Behaviour and design composite columns incorporating compact high-strength steel plates. *Journal of Constructional Steel Research, 107*, 94–110. https://doi.org/10.1016/j.jcsr.2015.01.005

Asteris, P. G., & Mokos, V. G. (2020). Concrete compressive strength using artificial neural networks. *Neural Computing and Applications, 32*, 11807–11826. https://doi.org/10.1007/s00521-019-04663-2

Avci-Karatas, C. (2021). Modeling approach for estimation of ultimate load capacity of concrete-filled steel tube composite stub columns based on relevance vector machine. *Nigde Omer Halisdemir University Journal of Engineering Sciences*. https://doi.org/10.28948/ngumuh.759297

Avci-Karatas, C. (2019). Prediction of ultimate load capacity of concrete-filled steel tube columns using multivariate adaptive regression splines (MARS). *Steel Compos Struct, 33*(4), 583–594. https://doi.org/10.12989/scs.2019.33.4.583

Avci-Karatas, C., Celik, O. C., & Eruslu, S. O. (2019). Modeling of buckling restrained braces (BRBs) using full-scale experimental data. *KSCE Journal of Civil Engineering, 23*(10), 4431–4444. https://doi.org/10.1007/s12205-019-2430-y

Avci-Karatas, C., Celik, O. C., & Yalcin, C. (2018). Experimental investigation of aluminum alloy and steel core buckling restrained braces (BRBs). *International Journal of Steel Structures, 18*(2), 650–673. https://doi.org/10.1007/s13296-018-0025-y

Beale, M. H., Hagan, M. T., & Demuth, H. B. (2010). *Neural network toolbox 7 user's guide*. Version R2011b, The MathWorks, Inc. 3 Apple Hill Drive Natick.

Behnood, A., & Golafshani, E. M. (2018). Predicting the compressive strength of silica fume concrete using hybrid artificial neural network with multi-objective grey wolves. *Journal of Cleaner Production, 202*(20), 54–64. https://doi.org/10.1016/j.jclepro.2018.08.065

Bianconi, A., Von Zuben, C. J., Serapião, A. B., & Govone, J. S. (2010). Artificial neural networks: A novel approach to analysing the nutritional ecology of a blowfly species, Chrysomya Megacephala. *Journal of Insect Science, 10*(58), 1536–2442. https://doi.org/10.1673/031.010.5801

Celik, O. C., Yuksel, E., Avci-Karatas, C., Bal, A., Gokce, T., Bago, Z., & Koller, G. (2015). Component testing of steel-core buckling restrained braces (BRBs) with pinned end connections. In *Proceedings of the 8th International Conference on Advances in Steel Structures (ICASS-2015)*.

Chalioris, C. E., Zapris, A. G., & Karayannis, C. G. (2020). U-jacketing applications of fiber-reinforced polymers in reinforced concrete T-beams against shear—tests and design. *Fibers, 8*(2), 13. https://doi.org/10.3390/fib8020013

Cheng, M. Y., & Cao, M. T. (2013). Evolutionary multivariate adaptive regression splines for estimating shear strength in reinforced-concrete deep beams. *Engineering Applications of Artificial Intelligence, 28*, 86–96. https://doi.org/10.1016/j.engappai.2013.11.001

Chithra, S., Kumar, S. R. R. S., Chinnaraju, K., & Alfin-Ashmita, F. (2016). A comparative study on the compressive strength prediction models for high performance concrete containing nano silica and copper slag using regression analysis and artificial neural networks. *Construction and Building Materials, 114*, 528–535. https://doi.org/10.1016/j.conbuildmat.2016.03.214

Demuth, H.B., Beale, M. H., & Hagan, M. T. (2006). *Neural network toolbox 5 user's guide*. Version 5, The MathWorks, Inc. 3 Apple Hill Drive Natick.

De Oliveira, W. L. A., De Nardin, S., de Cresce El, A. L. H., & El Debs, M. K. (2009). Influence of concrete strength and length/diameter on the axial capacity of CFT columns. *Journal of Constructional Steel Research, 65*(12), 2103–2110. https://doi.org/10.1016/j.jcsr.2009.07.004

Duan, Z. H., Kou, S. C., & Poon, C. S. (2013). Prediction of compressive strength of recycled aggregate concrete using artificial neural networks. *Construction and Building Materials, 40*, 1200–1206. https://doi.org/10.1016/j.conbuildmat.2012.04.063

Dutta, S., Murthy, A. R., Kim, D., & Samui, P. (2017). Prediction of compressive strength of self-compacting concrete using intelligent computational modelling. *Comput Mater Contin, 53*(2), 157–174. https://doi.org/10.3970/cmc.2017.053.167

Eurocode 4 (EC4): EN 1994-1-1. (2004). (English) *Design of composite steel and concrete structure—Part 1–1: General rules and rules for buildings* (pp. 117). CEN, Brussels: European Committee for Standardization. Authority: The European Union per Regulation 305/2011, Directive 98/34/EC, Directive 2004/18/EC]. https://eurocodes.jrc.ec.europa.eu/showpage.php?id=134.

Ekmekyapar, T., & Al-Eliwi, B. J. M. (2016). Experimental behaviour of circular concrete filled steel tube columns and design specifications. *Thin-Walled Structures, 105*, 220–230. https://doi.org/10.1016/j.tws.2016.04.004

Ellobody, E., Young, B., & Lam, D. (2006). Behavior of normal and high strength concrete-filled compact steel tube circular stub columns. *Journal of Constructional Steel Research, 62*(7), 706–715. https://doi.org/10.1016/j.jcsr.2005.11.002

Gallant, S .(1987). Automated generation of connectionist expert systems for problems involving noise and redundancy. In *Proceedings of the 3rd Conference on Uncertainty in Artificial Intelligence (UAI'87)* (pp. 212–221). ISBN: 978-0-444-87417-7.

Gardener, N. J., & Jacobson, R. (1967). Structural behavior of concrete filled steel tubes. *Journal of American Concrete Institute (ACI), 64*(7), 404–413.

Gardener, N. J. (1968). Use of spiral welded steel tubes in pipe columns. *Journal of American Concrete Institute (ACI), 65*(11), 937–942.

Gavin, H. P. (2013). *The Levenberg-Marquardt algorithm for nonlinear least squares curve-fitting problems*. Department of Civil and Environmental Engineering, Duke University.

Giakoumelis, G., & Lam, D. (2004). Axial capacity of circular concrete-filled tube columns. *Journal of Constructional Steel Research, 60*(7), 1049–1068. https://doi.org/10.1016/j.jcsr.2003.10.001

Ghamari, A., & Johari Naeimi, A. (2020). Investigating the seismic behaviour of high-performance steel plate shear walls. *Proceedings of the Institution of Civil Engineers-Structures and Buildings*. https://doi.org/10.1680/jstbu.20.00108

Gholampour, A., Mansouri, I., Kisi, O., & Ozbakkaloglu, T. (2020). Evaluation of mechanical properties of concretes containing coarse recycled concrete aggregates using multivariate adaptive regression splines (MARS), M5 model tree (M5Tree), and least squares support vector regression (LSSVR) models. *Neural Computing and Applications, 32*, 295–308. https://doi.org/10.1007/s00521-018-3630-y

Guler, S., Copur, A., & Aydogan, M. (2013). Axial capacity and ductility of circular UHPC-filled steel tube columns. *Mag Concrete Res, 65*(15), 898–905. https://doi.org/10.1680/macr.12.00211

Guler, S., Copur, A., & Aydogan, M. (2014). A comparative study on square and circular high strength concrete-filled steel tube columns. *Advanced Steel Construction, 10*(2), 234–247. https://doi.org/10.18057/IJASC.2014.10.2.7

Gupta, P. K., Sarda, S. M., & Kumar, M. S. (2007). Experimental and computational study of concrete filled steel tubular columns under axial loads. *Journal of Constructional Steel Research, 63*(2), 182–193. https://doi.org/10.1016/j.jcsr.2006.04.004

Han, L. H., & Yao, G. H. (2004). Experimental behaviour of thin-walled hollow structural steel (HSS) columns filled with self-consolidating concrete (SCC). *Thin-Walled Structures, 42*(9), 1357–1377. https://doi.org/10.1016/j.tws.2004.03.016

Han, L. H., Yao, G. H., & Zhao, X. L. (2005). Tests and calculations for hollow structural steel (HSS) stub columns filled with self-consolidating concrete (SCC). *Journal of Constructional Steel Research, 61*(9), 1241–1269. https://doi.org/10.1016/j.jcsr.2005.01.004

Han, L. H., Hou, C. C., & Wang, Q. L. (2014). Behavior of circular CFST stub columns under sustained load and chloride corrosion. *Journal of Constructional Steel Research, 103*, 23–36. https://doi.org/10.1016/j.jcsr.2014.07.021

Haque, M. E., & Sudhakar, K. V. (2002). ANN back-propagation prediction model for fracture toughness in microalloy steel. *International Journal of Fatigue, 24*(9), 1003–1010. https://doi.org/10.1016/S0142-1123(01)00207-9

Haykin, S. (1998). *Neural networks: A comprehensive foundation* (2nd ed.). Prentice Hall.

Hecht-Nielsen, R. (1989). *Neurocomputer Applications*. In: Eckmiller R., v.d. Malsburg C. (eds) Neural Computers. Springer Study Edition, vol 41. Springer. https://doi.org/10.1007/978-3-642-83740-1_45

Hoveidae, N., & Radpour, S. (2021). A novel all-steel buckling restrained brace for seismic drift mitigation of steel frames. *Bulletin of Earthquake Engineering*. https://doi.org/10.1007/s10518-020-01038-0

Huang, C. S., Yeh, Y. K., Liu, G. Y., Hu, H. T., Tsai, K. C., Weng, Y. T., Wang, S. H., & Wu, M. H. (2002). Axial load behavior of stiffened concrete-filled steel columns. *Journal of Structural Engineering (ASCE), 128*(9), 1222–1230. https://doi.org/10.1061/(ASCE)0733-9445(2002)128:9(1222)

Ince, R. (2004). Prediction of fracture parameters of concrete by artificial neural networks. *Engineering Fracture Mechanics, 71*(15), 2143–2159. https://doi.org/10.1016/j.engfracmech.2003.12.004

Johansson, M., & Gylltoft, K. (2002). Mechanical behavior of circular steel–concrete composite stub columns. *Journal of Structural Engineering (ASCE), 128*(8), 1073–1081. https://doi.org/10.1061/(ASCE)0733-9445(2002)128:8(1073)

Kamarthi, S. V., & Pittner, S. (1999). Accelerating neural network training using weight extrapolations. *Neural Networks, 12*(9), 1285–1299. https://doi.org/10.1016/S0893-6080(99)00072-6

Kaur, J., & Kaur, K. (2017). A fuzzy approach for an IoT-based automated employee performance appraisal. *Comput Mater Contin, 53*(1), 23–36.

Kitada, T. (1998). Ultimate strength and ductility of state-of-the-art concrete-filled steel bridge piers in Japan. *Engineering Structures, 20*(4–6), 347–354. https://doi.org/10.1016/S0141-0296(97)00026-6

Lam, D., & Gardner, L. (2008). Structural design of stainless steel concrete filled columns. *Journal of Constructional Steel Research, 64*(11), 1275–1282. https://doi.org/10.1016/j.jcsr.2008.04.012

Le, T. T. (2022). Practical machine learning-based prediction model for axial capacity of square CFST columns. *Mechanics of Advanced Materials and Structures*. https://doi.org/10.1080/15376494.2020.1839608

Lee, S. H., Uy, B., Kim, S. H., Choi, Y. H., & Choi, S. M. (2011). Behavior of highstrength circular concrete-filled steel tubular (CFST) column under eccentric loading. *Journal of Constructional Steel Research, 67*, 1–13. https://doi.org/10.1016/j.jcsr.2010.07.003

Levenberg, K. (1944). A method for the solution of certain problems in least squares. *Quarterly of Applied Mathematics, 2*(2), 164–168.

Liu, D. L., Gho, W. M., & Yuan, J. (2003). Ultimate capacity of high-strength rectangular concrete-filled steel hollow section stub columns. *Journal of Constructional Steel Research, 59*(12), 1499–1515. https://doi.org/10.1016/S0143-974X(03)00106-8

Liu, D. L., & Gho, W. M. (2005). Axial load behaviour of high-strength rectangular concrete filled steel tubular stub columns. *Thin-Walled Structures, 43*(8), 1131–1142. https://doi.org/10.1016/j.tws.2005.03.007

Lue, D. M., Liu, J. L., & Yen, T. (2007). Experimental study on rectangular CFT columns with high-strength concrete. *Journal of Constructional Steel Research, 63*(1), 37–44. https://doi.org/10.1016/j.jcsr.2006.03.007

Madsen, K., Nielsen, HB., & Tingleff, O. (2004). *Methods for non-linear least squares problems*. *Informatics and Mathematical Modelling (IMM)*. Technical University of Denmark, Lecture notes. Available at http://www.imm.dtu.dk/courses/02611/nllsq.pdf.

Mansouri, I., Kisi, O., Sadeghian, P., Lee, C. H., & Hu, J. W. (2017). Prediction of ultimate strain and strength of FRP-confined concrete cylinders using soft computing methods. *Applied Sciences, 7*(8), 751. https://doi.org/10.3390/app7080751

Mansouri, I., Safa, M., Ibrahim, Z., Kisi, O., Tahir, M. M., Baharom, S. B., & Azimi, M. (2016). Strength prediction of rotary brace damper using MLR and MARS. *Structural Engineering and Mechanics, 60*(3), 471–488. https://doi.org/10.12989/sem.2016.60.3.471

Marquardt, D. W. (1963). An algorithm for least-squares estimation of nonlinear parameters. *Journal of the Society for Industrial and Applied Mathematics, 11*(2), 431–441. https://doi.org/10.1137/0111030

Mittelmann, H. D. (2004). The Least Squares Problem. [web page] http://plato.asu.edu/topics/problems/nlolsq.html, Jul. 2004.

Murthy, A. R., Vishnuvardhan, S., Saravanan, M., & Gandhi, P. (2019). Relevance vector based approach for the prediction of stress intensity factor for the pipe with circumferential crack under cyclic loading. *Struct Eng Mech, 72*(1), 31–41. https://doi.org/10.12989/sem.2019.72.1.031

Ngo, N. T., Le, H. A., & Pham, T. P. T. (2021). Integration of support vector regression and grey wolf optimization for estimating the ultimate bearing capacity in concrete-filled steel tube columns. *Neural Computing and Applications*. https://doi.org/10.1007/s00521-020-05605-z

Osborne, M. R. (1992). Fisher's method of scoring. *Int. Stat. Rev., 86*, 271–286. https://doi.org/10.2307/1403504

O'Shea, M. D, Bridge, R. Q. (1994). Tests on thin-walled concrete-filled steel tubes. In *Proceedings of the 12th International Specialty Conference on Cold-Formed Steel Strucures* (pp. 399–419).

O'Shea, M. D., & Bridge, R. Q. (1998). Tests on circular thin-walled steel tubes filled with medium and high strength concrete. *Australian Civ. Eng. Trans., 40*, 15–27.

O'Shea, M. D., & Bridge, R. Q. (2000). Design of circular thin-walled concrete filled steel tubes. *J Struct Eng (ASCE)., 126*(11), 1295–1303. https://doi.org/10.1061/(ASCE)0733-9445(2000)126:11(1295)

Prasanna, P. K., Murthy, A. R., & Srinivas, K. (2018). Prediction of compressive strength of GGBS based concrete using RVM. *Struct Eng Mech, 68*(6), 691–700. https://doi.org/10.12989/sem.2018.68.6.691

Roshan, P. R. (2007). *Predicting bid prices in construction projects using non-parametric statistical models*. Master of Science in Civil Engineering Thesis, A&M University.

Sakino, K., & Hayashi, H. (1991). Behavior of concrete filled steel tubular stub columns under concentric loading. In *Proceedings of the 3rd International Conference on Steel Concrete Composite Structures* (pp. 25–30).

Sakino. K., & Sun, Y. (2000). Steel jacketing for improvement of column strength and ductility. In *Proceedings of the 12th World Conference on Earthquake Engineering*.

Sakino, K., Nakahara, H., Morino, S., & Nishiyama, I. (2004). Behavior of centrally loaded concrete-filled steel-tube short columns. *Journal of Structural Engineering (ASCE), 130*(2), 180–188. https://doi.org/10.1061/(ASCE)0733-9445(2004)130:2(180)

Schneider, S. P. (1998). Axially loaded concrete-filled steel tubes. *Journal of Structural Engineering (ASCE), 124*(10), 1125–1138. https://doi.org/10.1061/(ASCE)0733-9445(1998)124:10(1125)

Soman, M., & Chandrakumar, C. R. (2018). Axial behaviour of glass fibre reinforced polymer-confined reinforced concrete short columns. *Structural Engineering International, 28*(1), 44–50. https://doi.org/10.1080/10168664.2018.1431422

Talyan, N., Elias, S., & Matsagar, V. (2021). Earthquake response control of isolated bridges using supplementary passive dampers. *Practice Periodical on Structural Design and Construction, 26*(2), 04021002. https://doi.org/10.1061/(ASCE)SC.1943-5576.0000563

Tan, K. F., Pu, X. C., & Cai, S. H. (1999). Study on the mechanical properties of steel extra-high strength concrete encased in steel tubes. *Journal of Building Structures, 20*(1), 10–15.

Tomii, M., Yoshimura, K., & Morishita, Y. (1977). Experimental studies on concrete filled steel tubular stub columns under concentric loading. In *Proceedings of the International Colloquium on Stability of Structures Under Static and Dynamic Loads* (pp. 718–741).

Uy, B. (2001). Strength of short concrete filled high strength steel box columns. *Journal of Constructional Steel Research, 57*(2), 113–134. https://doi.org/10.1016/S0143-974X(00)00014-6

Xiong, M. X., Xiong, D. X., & Liew, J. Y. R. (2017). Axial performance of short concrete filled steel tubes with high- and ultra-high- strength materials. *Engineering Structures, 136*, 494–510. https://doi.org/10.1016/j.engstruct.2017.01.037

Yamamoto, T., Kawaguchi, J., & Morino, S. (2002). Experimental study of scale effects on the compressive behavior of short concrete-filled steel tube columns. In P*roceedings of the United Engineering Foundation Conference on Composite Construction in Steel and Concrete IV (AICE)* (pp. 879–890).

Yu, Z. W., Ding, F. X., & Cai, C. S. (2007). Experimental behavior of circular concretefilled steel tube stub columns. *Journal of Constructional Steel Research, 63*, 165–174. https://doi.org/10.1016/j.jcsr.2006.03.009

Yu, Q., Tao, Z., & Wu, Y. X. (2008). Experimental behaviour of high performance concrete filled steel tubular columns. *Thin Walled Structures, 46*(4), 362–370. https://doi.org/10.1016/j.tws.2007.10.001

Yuvaraj, P., Murthy, A. R., Iyer, N. R., Samui, P., & Sekar, S. K. (2013). Multivariate adaptive regression splines model to predict fracture characteristics of high strength and ultra high strength concrete beams. *CMC: Computers, Materials and Continua, 36*(1), 73–97. https://doi.org/10.3970/cmc.2013.036.073

Yuvaraj, P., Murthy, A. R., Iyer, N. R., Samui, P., & Sekar, S. K. (2014). Prediction of fracture characteristics of high strength and ultra high strength concrete beams based on relevance vector machine. *International Journal of Damage Mechanics, 23*(7), 979–1004. https://doi.org/10.1177/1056789514520796